*infrastructures*

MDPI

*Article*

# Predictive Analysis of Corrosion Dynamics in Prestressed Concrete Exposed to Chloride Environments

**Rodrigo Moulin Ribeiro Pierott [1,*], Sergio Garcia [2], Diogo Kropf [2], Karoline Figueiredo [1], Bruno Barzellay Ferreira da Costa [1], Mayara Amario [1], Mohammad K. Najjar [1] and Assed Haddad [1,*]**

[1] Environmental Engineering Program, Federal University of Rio de Janeiro, Rio de Janeiro 21941-630, Brazil; karolinefigueiredo@poli.ufrj.br (K.F.); bruno.barzellay@macae.ufrj.br (B.B.F.d.C.); mayara_amario@poli.ufrj.br (M.A.); mnajjar@poli.ufrj.br (M.K.N.)

[2] Civil Engineering Program, State University of North Fluminense, Campos dos Goytacazes 28013-602, Brazil; liluiser@uenf.br (S.G.); diogokropf@isecensa.edu.br (D.K.)

* Correspondence: rpierott@poli.ufrj.br (R.M.R.P.); assed@poli.ufrj.br (A.H.)

**Abstract:** This study investigates the corrosion behavior of 5 mm diameter prestressed wires in concrete beams under chloride attack, a prevalent issue for coastal infrastructure. The study simulated aggressive chloride environments to understand their impact on structural integrity and service life. Utilizing a combination of advanced digital image correlation (DIC) techniques and a novel machine learning-based predictive model, the research provides a nuanced analysis of the interplay between stress levels, corrosion rates, and concrete strength. Empirical findings reveal a significant correlation between increased prestress levels and accelerated corrosion, indicating a crucial consideration for the design and maintenance of prestressed concrete structures. Notably, this study found that beams with a 95% prestress level exhibited a corrosion rate of 0.64 mm/year, significantly higher than the 0.37 mm/year for non-prestressed beams. The predictive model's accuracy was validated with a mean squared error of 0.517 and an $R^2$ value of 0.905, offering a valuable tool for quantifying the impact of corrosion. Therefore, the predictive model is a valuable tool for quantifying the impact of corrosion, enhancing the ability to assess and improve the durability of such infrastructure. This study's insights highlight the necessity for a balanced approach to design and regular monitoring, especially in chloride-rich environments. By helping to develop more resilient construction practices and contributing to sustainable development goals, this study can significantly impact the safety and service life of coastal bridges and structures, aligning with global efforts to create more sustainable and durable infrastructure.

**Keywords:** prestressed concrete; corrosion dynamics; structural integrity; predictive modeling

check for updates

**Citation:** Pierott, R.M.R.; Garcia, S.; Kropf, D.; Figueiredo, K.; da Costa, B.B.F.; Amario, M.; Najjar, M.K.; Haddad, A. Predictive Analysis of Corrosion Dynamics in Prestressed Concrete Exposed to Chloride Environments. *Infrastructures* **2024**, *9*, 133. https://doi.org/10.3390/infrastructures9080133

Academic Editor: Chris Goodier

Received: 26 June 2024
Revised: 2 August 2024
Accepted: 7 August 2024
Published: 10 August 2024

**Copyright:** © 2024 by the authors. Licensee MDPI, Basel, Switzerland. This article is an open access article distributed under the terms and conditions of the Creative Commons Attribution (CC BY) license (https://creativecommons.org/licenses/by/4.0/).

## 1. Introduction

The deterioration of prestressed concrete structures in chloride-rich environments due to corrosion is a significant concern, affecting both the service life and safety of such infrastructure. This issue is crucial for civil and environmental engineering, where the degradation of infrastructure due to corrosion represents not only a safety hazard but also a substantial environmental and economic burden [1,2]. Recent studies have highlighted the use of advanced materials and coatings to mitigate corrosion, improving the durability of these structures in aggressive environments [3]. This issue is crucial for civil and environmental engineering, where the degradation of infrastructure due to corrosion represents not only a safety hazard but also a substantial environmental and economic burden. The corrosion of steel reinforcement in concrete structures significantly impacts their serviceability, safety, and service life, necessitating a comprehensive understanding of corrosion mechanisms and their impacts on developing sustainable civil engineering practices.

Previous studies highlighted the severe consequences of corrosion in concrete structures. Ref. [4] noted that corrosion leads to cracking, bond strength reduction, and structural integrity loss, emphasizing the necessity of understanding corrosion rates to predict serviceability loss. Similarly, Ref. [5] explored steel corrosion mechanisms, particularly carbonation and chloride penetration, and discussed approaches for designing durable structures to extend their service life in aggressive environments. Additionally, the effectiveness of electrochemical repair methods and the performance of corrosion inhibitors were extensively studied, providing insights into the long-term protection of concrete structures against corrosion stimulation [6,7]. Recent advances in mechanical–transport–chemical modeling further enhanced our ability to evaluate the effectiveness of electrochemical repair methods for corrosion-induced cracking in concrete structures, providing a robust framework for optimizing repair techniques and improving durability [1]. Moreover, the broader environmental implications associated with resource utilization, energy consumption, and emissions from manufacturing and construction activities further underscore the importance of addressing this issue [8].

The necessity of developing sustainable practices in civil engineering is evident, as discussed by [3], highlighting the importance of corrosion protection in sustainable energy systems and infrastructure. Another study reviewed the use of ionic liquids as sustainable corrosion inhibitors, emphasizing their potential to reduce environmental impacts and enhance material service life [9]. Furthermore, the application of artificial neural networks (ANNs) in predicting chloride diffusivity in concrete has shown promising results, enhancing the accuracy and robustness of corrosion modeling under various environmental conditions [2].

While many documented cases of corrosion pertain to post-tensioned members, pretensioned members are also susceptible to corrosion, especially in chloride-rich environments. The literature includes instances of failures due to corrosion in pre-tensioned members, highlighting the need for focused research in this area.

Research shows that prestressed concrete structures, particularly those containing 5 mm diameter wires, are highly susceptible to accelerated corrosion in chloride-laden environments, increasing the risk of structural collapse compared to reinforced concrete [10]. Besides, models predicting the flexural strength of partially prestressed concrete structures emphasize the critical nature of corrosion in such environments [11]. In this context, methodologies for predicting the corrosion-free service life of concrete structures exposed to chlorides underscore the importance of regular maintenance and evaluation to prevent corrosion-related failures [12].

Despite this growing discussion, there remains a critical gap in understanding the specific corrosion dynamics in prestressed concrete [13], especially for smaller-diameter wires. Addressing this gap is essential for developing effective prevention and mitigation strategies that enhance structural service life and safety [14].

Therefore, this study explicitly simulates the aggressive chloride environments to replicate the corrosive conditions faced by coastal infrastructure closely. By focusing on the corrosion behaviors of prestressed concrete beams used in bridges and other coastal structures, this study aims to provide direct implications for such infrastructure's maintenance, design, and service life.

To achieve this goal, this study investigates the corrosion behavior of 5 mm diameter prestressed wires in chloride environments through a combination of empirical analysis and predictive modeling. This study uses advanced digital image correlation (DIC) techniques and a novel machine learning-based predictive model to analyze the interplay between stress levels, corrosion rates, and concrete strength.

To complement the experimental investigation of corrosion in prestressed concrete beams, we employed statistical and machine learning techniques to analyze the relationship between key variables and predict the structural integrity of the beams. These techniques provide a robust framework for understanding interactions and enhancing predictive accuracy.

Ultimately, the novelty of this research is its direct contribution to developing more durable and environmentally sustainable construction materials and methods, enhancing the safety and integrity of concrete structures, and supporting the global movement towards environmentally responsible civil engineering practices.

## 2. Background

Corrosion in prestressed concrete primarily results from chloride ion penetration, which is prevalent in corrosive environments. When chloride ions breach the concrete cover and reach the steel reinforcement, it leads to the formation of rust. This process expands the volume of the steel, causing cracking and spalling of the concrete cover and reducing the effective cross-sectional area of the reinforcement. Notably, [15] demonstrated that the loss of beam section and the breakage of prestressed steel strands due to corrosion significantly reduce beam stiffness and structural integrity.

Recent advancements in digital image correlation (DIC) technology and machine learning havesignificantly enhanced the ability to analyze and predict corrosion behavior in concrete structures. DIC technology provides high-resolution and non-contact measurement of surface deformation, enabling detailed monitoring of crack formation and propagation. Meanwhile, machine learning algorithms offer powerful tools for predictive modeling, capable of identifying complex patterns and relationships within large datasets to forecast corrosion impact with high accuracy.

In addition, experimental studies have provided insights into how corrosion affects the mechanical performance of prestressed concrete beams. For example, two different studies investigated the flexural performance of post-tensioned beams under different corrosion and grouting conditions. These studies found that corrosion decreased the flexural capacity and altered the crack patterns and load-deflection responses [16,17]. Additionally, [18] conducted experiments to evaluate the bending characteristics and bearing capacities of corroded beams, highlighting the critical role of corrosion rates in determining the extent of structural degradation. In a similar manner, [19] provided an overview of modeling corrosion in steel and reinforced concrete and highlighted the role of environmental factors. Finally, [20] developed a finite-element framework to evaluate the effects of various exposure conditions on corrosion, demonstrating the significance of integrating environmental stressors in predicting structural durability.

Over time, several empirical models have been developed to predict the residual flexural capacity of corroded prestressed concrete beams. These models typically consider factors such as sectional area loss, mechanical property degradation, grouting defects, and bond deterioration due to corrosion. For instance, [17] proposed models that incorporate the reduction in the cross-sectional area of the steel reinforcement and the degradation of mechanical properties due to corrosion. Likewise, [21] proposed a method using machine learning to predict the service life of reinforced concrete structures. Additionally, [18] developed a model that evaluates the cooperative behavior between corroded steel and concrete, providing a comprehensive understanding of how corrosion impacts the structural integrity of prestressed concrete beams. However, these models exhibit varying degrees of accuracy and often require calibration against experimental data to ensure reliability.

In this context, the development of non-destructive testing techniques advanced the ability to detect and monitor corrosion in prestressed concrete structures. For example, a study published in 2013 explored the use of acoustic emission (AE) techniques for early-stage corrosion detection and crack classification [22], while [23] presented a review of the advances in the use of sensors for reinforcement corrosion monitoring. Their research demonstrated the effectiveness of AE in identifying corrosion, macrocracks, and crack propagation, providing a valuable tool for structural health monitoring and proactive maintenance.

Nonetheless, the recent literature underscores the complexity of corrosion dynamics in corrosive environments for prestressed concrete structures. While our understanding of the mechanisms and impacts of corrosion and developing predictive models have come a

long way, challenges remain in ensuring the accuracy and applicability of these models across diverse environmental conditions. The integration of advanced monitoring techniques, such as AE, offers promising avenues for enhancing the detection and mitigation of corrosion-related damage, ultimately contributing to the durability and safety of coastal infrastructure.

## 3. Proposed Methods

The computational methodology component complements the experimental research by providing detailed analysis through computer-based modeling and simulations. This includes the EDA process, visual insights, model validation, and mathematical equations, as presented in Figure 1. Therefore, this study proposes processing the experimental data using statistical and computational techniques to identify patterns and correlations between stress levels, corrosion rates, and concrete strength. Based on the findings, a machine learning-based predictive model is developed to quantify the impact of corrosion. This model should be trained on the empirical data obtained from the experiments and validated through cross-validation techniques to ensure accuracy and reliability.

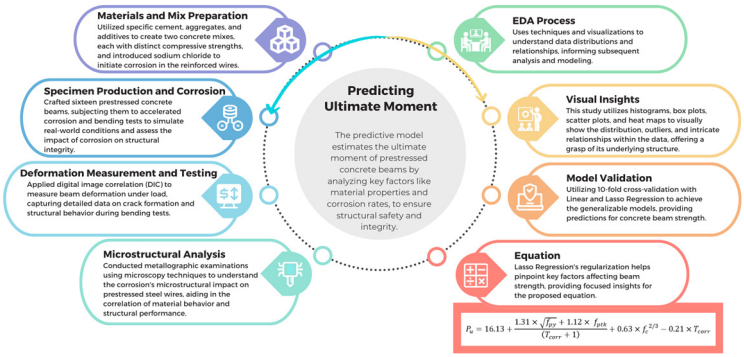


**Figure 1.** Proposed methodology of the study.

The proposed methodology for this study is divided into two main components: experimental research and computational methodology. In the experimental research component, this study proposes a series of practical experiments focusing on the behavior of prestressed concrete beams under chloride attack. This involves several steps, as follows: (i) material and mix preparation, (ii) specimen production and corrosion, (iii) microstructural analysis, and (iv) deformation measurement and testing [24,25]. Thus, a thorough understanding of corrosion mechanisms [26] and their impact on concrete structures is crucial for advancing sustainable civil engineering practices aimed at reducing both the environmental footprint and ensuring structural safety [27].

This study focuses on the corrosion of prestressed concrete structures, particularly on the behavior of 5 mm diameter prestressed wires in chloride environments. While there is extensive research on corrosion in reinforced concrete, studies specifically addressing prestressed concrete are limited. Prestressed structures, due to their unique design and material properties, often exhibit different, sometimes more severe, corrosion responses compared to reinforced structures [22]. The collapse of the Ynys-y-Gwas bridge in the UK and the recent and notable example of the catastrophic impact of corrosion on prestressed concrete structures, the collapse of the Morandi Bridge in Italy in 2018, underscore the critical need to understand the specific corrosion dynamics in prestressed concrete, particularly in smaller diameter wires. The utility of guided ultrasonic waves in inspecting embedded tendons in post-tensioned bridges, a method driven by the necessity to prevent incidents like the Ynys-y-Gwas bridge collapse, was emphasized by [28]. These studies collectively stress the urgency of developing effective corrosion prevention strategies for prestressed concrete structures to avoid catastrophic failures.

From an environmental standpoint, the significance of this research is twofold. Extending the lifespan of concrete structures through better understanding and prevention of corrosion formation can significantly reduce the need for frequent repairs and reconstructions [29], thereby minimizing the related environmental impacts. This approach is aligned with sustainable civil engineering principles, which emphasize durable and low-impact construction practices. Moreover, our study contributes to the critical knowledge base needed for the shift towards more sustainable construction practices. It underscores the possibilities for innovative designs and material choices that not only improve structural durability but also contribute to environmental conservation.

In exploring the corrosion behavior of prestressed wires in chloride environments, this study aims to offer insights that could lead to advancements in both material science and construction methodologies. These advancements are expected to profoundly impact the field of civil engineering, contributing to the development of infrastructure that is more resilient and more in harmony with our environmental responsibilities.

## 4. Materials

This study utilized high-early-strength Portland cement (CPV ARI) with a density of 3100 kg/m$^3$ and Blaine fineness of 470 kg/m$^2$. Basalt-type coarse aggregate (unit weight of 2.73 g/cm$^3$ and bulk density of 1.58 g/cm$^3$) and natural quartz sand (unit weight of 2.63 g/cm$^3$ and bulk density of 1.54 g/cm$^3$) were chosen for their compatibility and performance. Silica fume (density of 2.20 g/cm$^3$) and a superplasticizer based on modified carboxylic ether (density of 1.070 g/cm$^3$, pH 6) were also incorporated. The superplasticizer facilitated high water removal rates, ensuring workability without altering the setting time. The reinforcement used in the prestressed beams comprised notched ribbed CP-175 RB 5 wire, with a diameter of 5.0 mm and a tensile strength of 1860 MPa, as established through preliminary tensile tests and highlighted in Figure 2.

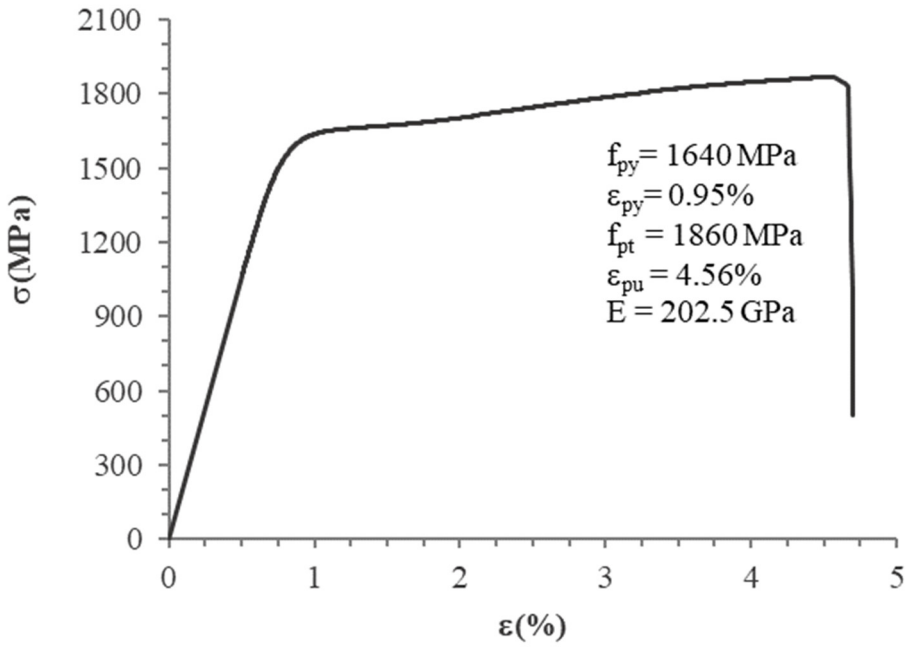


**Figure 2.** Stress versus strain of the prestressed reinforcement.

### *4.1. Concrete Proportions*

Two concrete mixes were prepared with target compressive strengths of 32 MPa and 68 MPa, with subsequent testing to measure the actual compressive strengths for use in structural analyses. The 32 MPa mix had a 1:2.25:3.25 cement/sand/coarse aggregate ratio, 0.58 w/c ratio, and an 80 mm slump. The 68 MPa mix was denser with a 1:0.94:1.89 ratio, 0.34 w/c ratio, 0.25 water/cementitious material factor, plus 0.5% superplasticizer and 10%

silica fume, achieving a 90 mm slump. Both mixes included 2% sodium chloride (NaCl) by cement weight to initiate corrosion, as per Mancini et al. (2014). Material volumes are presented in Table 1.

**Table 1.** Amount of material used per $m^3$ of concrete in the beams tested.

| Materials | 32 MPa ($kg/m^3$) | 68 MPa ($kg/m^3$) |
|---|---|---|
| Portland cement | 329 | 550 |
| Sand | 740 | 520 |
| Gravel | 1069 | 1043 |
| Water | 191 | 154 |
| Silica fume | - | 55 |
| Superplasticizer | - | 2.78 |
| NaCl | 6.58 | 11 |

### *4.2. Specimen Details and Casting*

Sixteen prestressed concrete beams (150 × 300 × 1500 mm) underwent three-point bending tests, as illustrated in Table 2. Classified as VX-Y-Z (X = concrete strength, Y = wire stress, Z = corrosion status), they varied in prestress and strength levels. Half had non-corroded (NCB), and half had corroded pre-cracked wires (CB). Beams were cast in a 3 m formwork, producing six at a time, using a hydraulic system for prestressing. After a 24 h demolding period, they were wet-cured for 28 days. The anchoring system of the prestressed wire and the metal formwork for concreting the prestressed beams are presented in Figure 3 and Figure 4, respectively.

**Table 2.** Specimen details.

| Samples | Compressive Strength (MPa) | Stress Level | Cl- Concentration | Pre-Tension (MPa) | Replica |
|---|---|---|---|---|---|
| V32-0-Z. | 32 | 0% $f_{ptk}$ | 2 | 0 | 2 |
| V32-0.5-Z | | 50% $f_{ptk}$ | 2 | 930 | 2 |
| V32-0.7-Z | | 70% $f_{ptk}$ | 2 | 1302 | 2 |
| V32-0.95-Z | | 95% $f_{ptk}$ | 2 | 1767 | 2 |
| V68-0-Z | 68 | 0% $f_{ptk}$ | 2 | 0 | 2 |
| V68-0.5-Z | | 50% $f_{ptk}$ | 2 | 930 | 2 |
| V68-0.7-Z | | 70% $f_{ptk}$ | 2 | 1302 | 2 |
| V68-0.95-Z | | 95% $f_{ptk}$ | 2 | 1767 | 2 |

The cross section of the beam models included four prestressed steel wires, positioned symmetrically around the neutral axis, with two wires in the upper layer and two in the lower layer, ensuring the uniform distribution of prestressing forces.

We acknowledge that the a/d ratio used in the tests is below 5, indicating significant shear in addition to bending. Future studies in this area will need to adjust the beam model proportions to ensure a/d ratios above 5 and span-to-height ratios over 20 to better isolate bending effects.

In Table 2, the chloride concentration in the concrete was controlled by adding a specified amount of sodium chloride (NaCl) to the mix during the preparation phase, ensuring consistent chloride content across samples.

The experimental setup expedited the corrosion of prestressed steel wires in concrete beams, beginning after a 28-day wet curing period. The purpose of this acceleration was to replicate natural corrosion rapidly and under controlled laboratory conditions, facilitating an in-depth study of its effects.



**Figure 3.** Anchoring system of the prestressed wire.

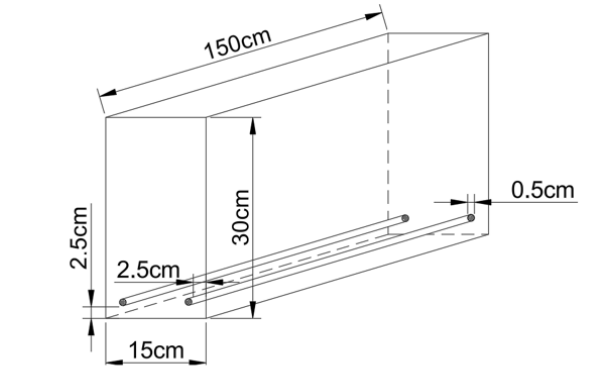




**Figure 4.** Cross section of the beam, measuring 30 cm in height, 15 cm in width, 150 cm in length, and containing two reinforcements with a diameter of 0.5 cm. The metal formwork for casting multiple prestressed beams each time is also shown.

Corrosion was induced using a sophisticated electrochemical setup comprising four direct current (DC) power supplies connected in series. This system provided a range of 12 to 30 volts, enabling a current of up to 1 ampere and a maximum voltage of 66 volts. Beams with a higher compressive strength of 68 MPa required this increased voltage to achieve significant current levels for corrosion, compared to their 32 MPa counterparts.

In this setup, the prestressed steel wire within each beam was the anode, connected to the positive terminal of the power supply. This connection caused the wire to undergo accelerated oxidation, simulating the natural rusting process at a much faster rate. A less electronegative plate, introduced during casting and connected to the negative terminal, acted as the cathode, where reduction reactions typically occurred.

This controlled electrochemical environment within each beam led to an accelerated onset and progression of corrosion on the steel wires. To monitor this process, corrosion potential (Ecorr) readings were systematically taken. Using two multimeters, the current for each beam and Ecorr were recorded at 15 strategic points along the wire's length, providing a detailed map of corrosion progression.

Over 168 h, Ecorr readings were continuously recorded every 24 h. These readings showed significant potential differences, with −730 mV for 32 MPa beams and −510 mV for 68 MPa beams at 95% fptk pre-tension of the wires, indicating varying corrosion rates and initiation points across different beam types. Figures 5–7 show the beams connected to the power supplies and the corresponding Ecorr readings, illustrating the comprehensive monitoring and analysis carried out in this study.



**Figure 5.** Current applied to the beams being recorded by multimeters.

Precise monitoring and control of the accelerated corrosion process were important to accurately mimic real-world scenarios in prestressed concrete beams. This method provided insight into how concrete strength and prestressing levels affect steel wire corrosion.

### *4.3. Instrumentation*

This study measured beam deformation during bending tests using digital image correlation (DIC), a non-contact optical metrology technique providing detailed deformation and strain measurements. Beam surfaces were prepared with a high-contrast speckle pattern for effective DIC tracking, as shown in Figure 6. Cameras captured images before and after load application, and the DIC software analyzed the displacement and strain by tracking speckle movements, creating a detailed deformation map (Figure 6). This precise method offered a comprehensive understanding of the beam's behavior under stress, enhancing the study's insights into beam response under bending loads.

### *4.4. Digital Image Correlation (DIC)*

The experimental phase included measuring beam deformation during bending tests using digital image correlation (DIC), a non-contact optical method that extensively measures and visualizes material deformation and strain. The beams were prepared with a white base layer and black speckles to enhance the DIC system's tracking accuracy. This preparation allowed the DIC software to precisely correlate changes before and after load application, providing crucial data on beam displacement and deformation (Figure 6).

The models were tested to the point of failure. The observed failure modes included significant flexural cracking followed by concrete crushing in the compression zone and bond failure between the prestressed steel and concrete due to corrosion.




**Figure 6.** Area selected for displacement analysis.

After preparing the beams, two cameras captured images from different angles for digital image correlation (DIC) analysis. The DIC system compared pre- and post-load images to track speckle movements and calculate beam displacement and strain. This process produced a detailed strain distribution pattern for the loaded beam (Figure 6).

### *4.5. Bending Test Procedure*

The bending tests involved 1500 mm long beams with a 1400 mm span between supports. Subjected to a three-point loading configuration to assess flexural strength and behavior, these tests formed a critical part of the experimental research (Figure 7).

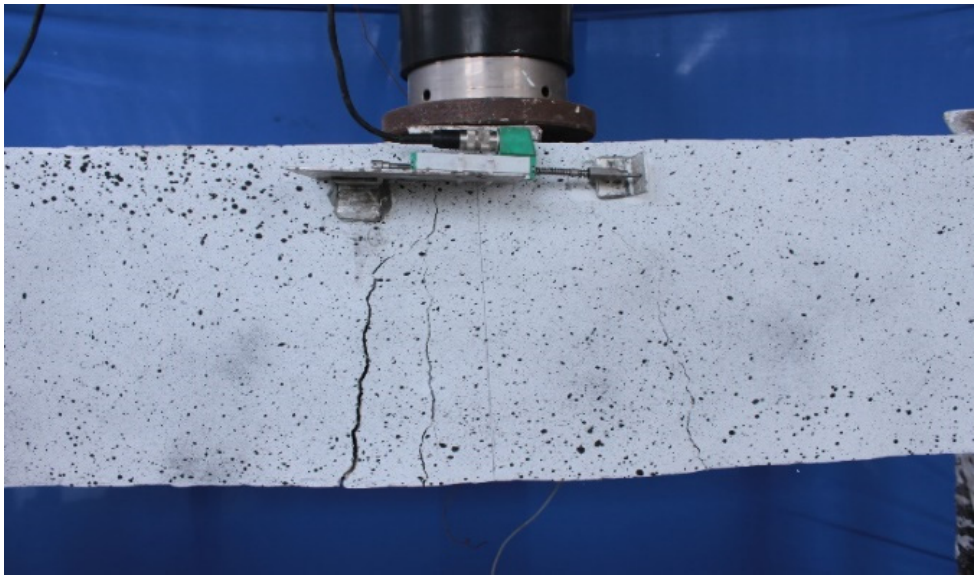

**Figure 7.** Cracks in beam V32-0.5-NCB.

The bending tests were performed at the UENF Civil Engineering Laboratory using a robust testing setup. This setup included a metal frame and a high-capacity hydraulic actuator, specifically an MTS® 244.41 model. The hydraulic actuator, coupled with a 500 kN capacity load cell, applied the load to the beams. The load was applied monotonically at a controlled rate of 0.1 mm/min. This slow and steady rate of loading was important for accurately observing the progression of cracks and other failure modes in the beams.

The cross section of the beam models included four prestressed steel wires, positioned symmetrically around the neutral axis, with two wires in the upper layer and two in the lower layer, ensuring a uniform distribution of prestressing forces. The deformation along the cross-section at mid-span in the 32 MPa beams is illustrated in Figure 8, while the bending crack pattern of the specimens is presented in Figure 9.

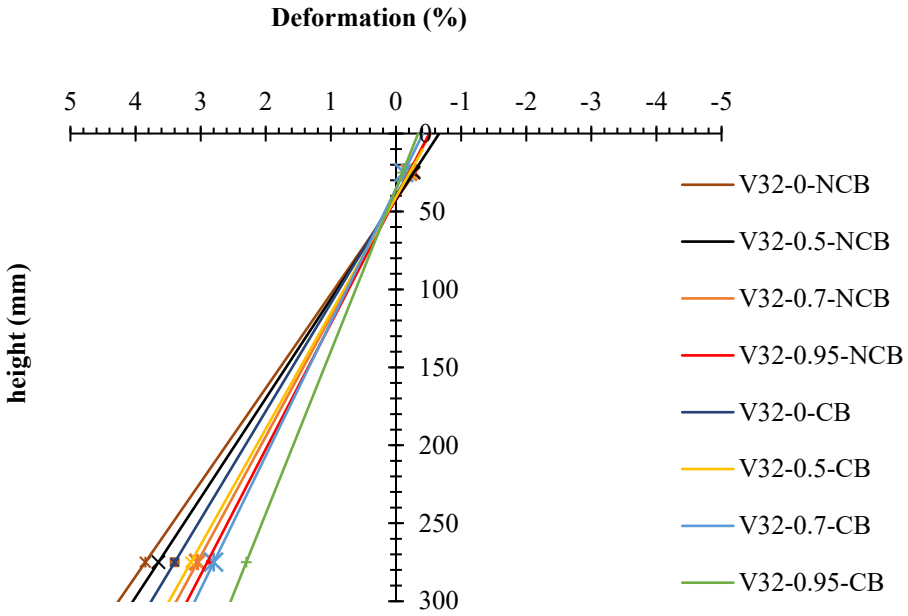


**Figure 8.** Deformation along the cross-section at mid-span in the 32 MPa beams.

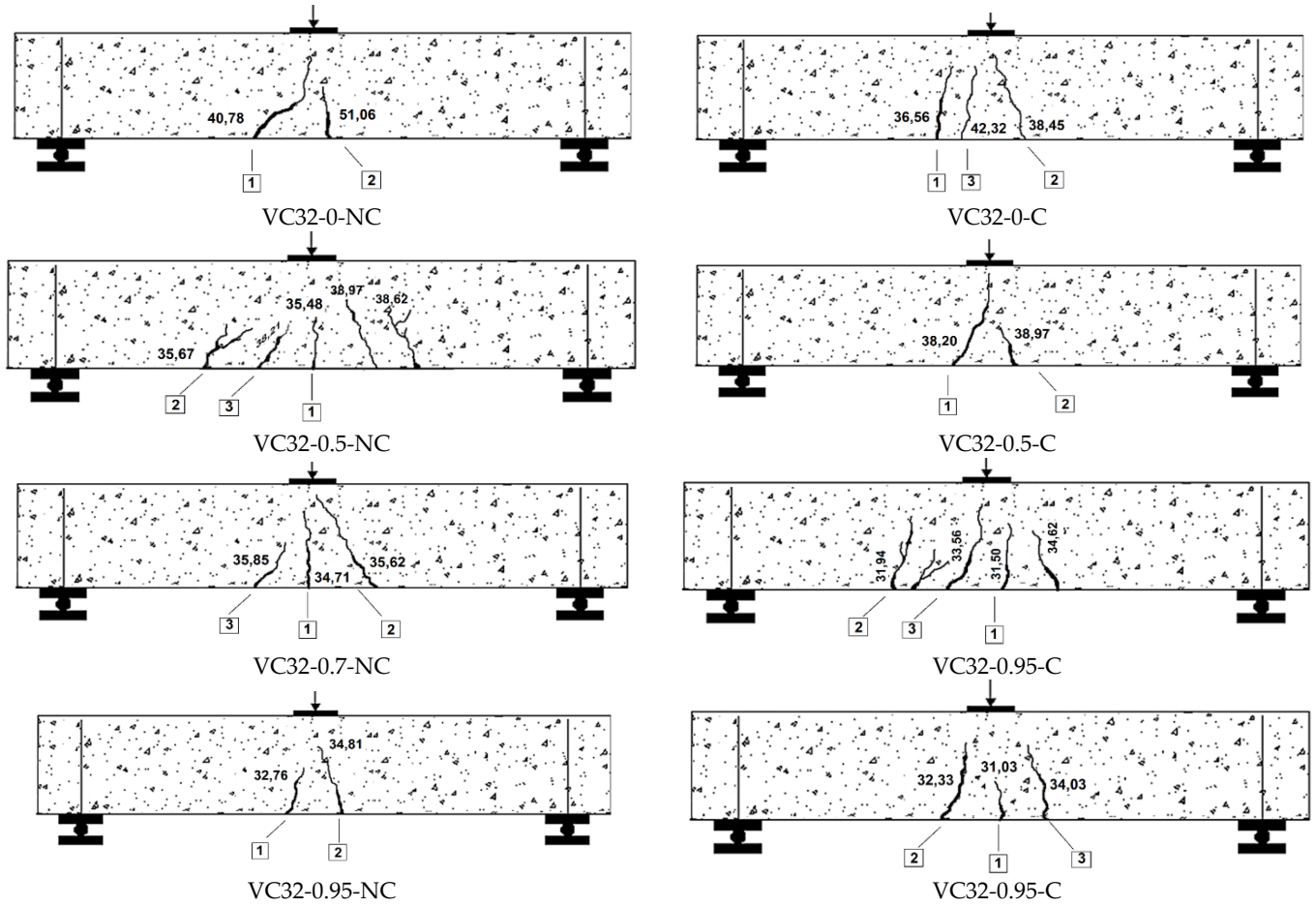


**Figure 9.** Bending crack pattern of the specimens.

In Figure 9, the numbers on the beam indicate the measured fracture widths in millimeters, highlighting areas of significant stress concentration where the most severe cracks developed.

All of the beams failed due to excessive deformation of the prestressed longitudinal reinforcement, demonstrating structural ductility.

As the load was applied, the beams were closely monitored for any signs of cracking, deformation, or ultimate failure. The DIC system played a pivotal role in this phase, providing real-time data on the deformation patterns of the beams. This data was essential for understanding how the corrosion of the prestressed wires affected the structural behavior of the beams, particularly in terms of crack formation, propagation, and the overall flexural performance. The corrosion rate versus rupture deformation is simulated in Figure 10.

Figure 10 presents the corrosion rate versus rupture deformation. The data illustrate the relationship between measured corrosion rates and the deformation at rupture of the beams, indicating how increased corrosion accelerates the reduction in deformation capacity.

The combination of the DIC instrumentation and the controlled bending test setup allowed for a comprehensive analysis of the impact of corrosion on the prestressed concrete beams. The data gathered provided insights into the changes in mechanical properties due to corrosion, contributing significantly to the study's findings on the durability and resilience of prestressed concrete structures in corrosive environments.

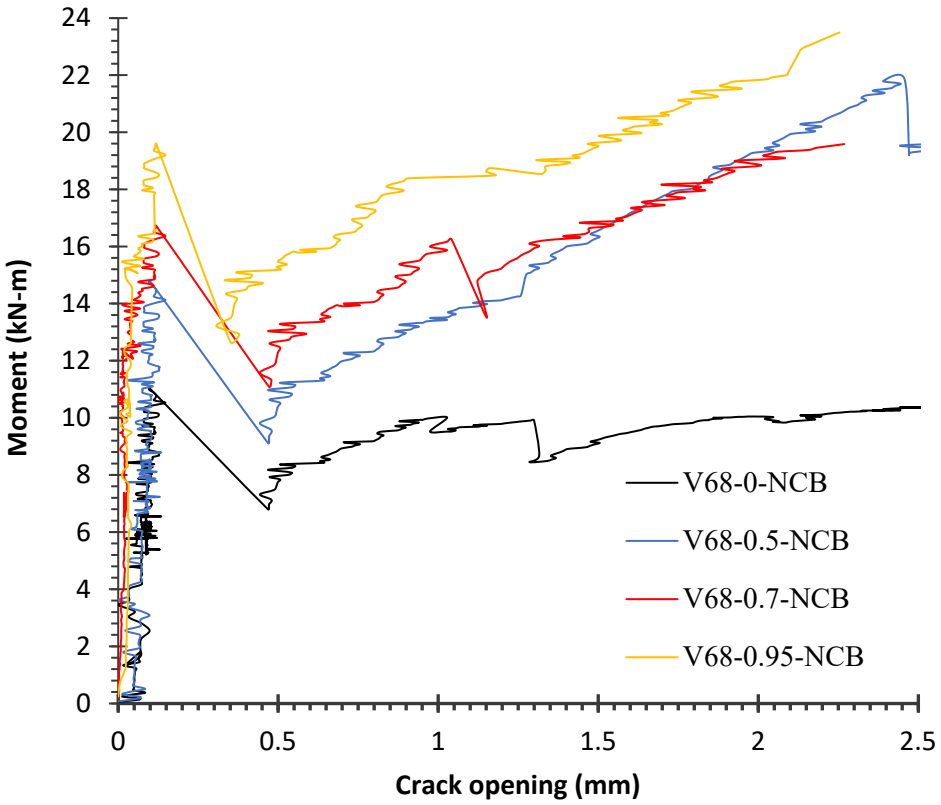


**Figure 10.** Corrosion rate versus rupture deformation.

### *4.6. Metallographic Characterization of the Wires*

The metallographic characterization of the prestressed steel wires was part of the experimental research, as it provided critical insights into the microscopic changes and damage mechanisms caused by corrosion [30]. This characterization involved a series of analyses using optical microscopy, confocal microscopy, and scanning electron microscopy (SEM). These techniques were instrumental in identifying and understanding the microstructural alterations in the wires due to corrosion processes. Figures 11 and 12 illustrate the significant differences in corrosion morphology and potential for both 32 MPa and 68 MPa beams.

Before the microscopic examination, the prestressed wires were carefully extracted from the concrete beams to preserve the integrity of the corrosion layer. This extraction was carried out meticulously to avoid any additional mechanical damage that could interfere with the accuracy of the metallographic observations.

### *4.7. Optical Microscopy Analysis*

The initial examination was conducted using optical microscopy. This phase involved observing the cross-section of the corroded wires from the 32 MPa and 68 MPa beams. In the optical microscopy images (Figure 11), a distinction was evident between the dark and light regions, representing the embedding product of the sample and the intact wire, respectively. A key observation was the identification of areas with corrosive characteristics between the embedding product and the wire, indicating the extent and nature of the corrosion [31]. The full perimeter of the wire was analyzed to assess the uniformity of corrosion and identify any surface layer loss, characterized by protrusions and indentations. The corrosion potential is illustrated in Figure 12.

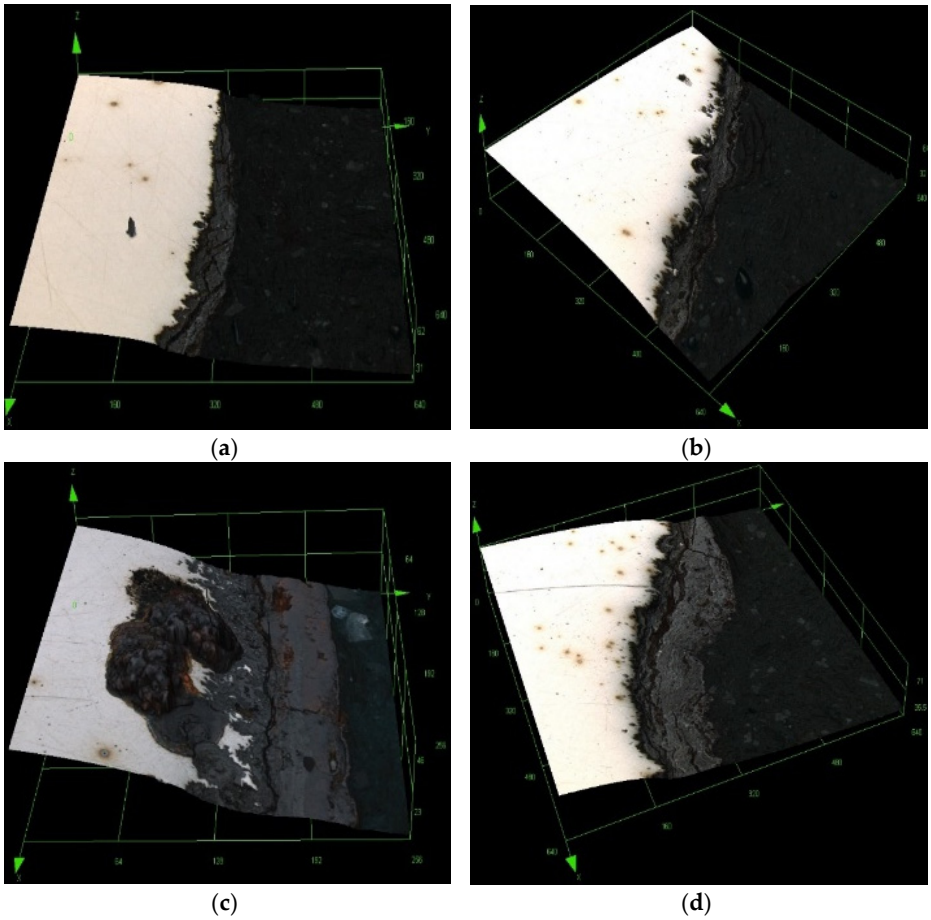


**Figure 11.** Optical microscopy images of corrosion from the environment of 32 MPa beams at different stress levels: (**a**) V32-0-CB; (**b**) V32-0.5-CB; (**c**) V32-0.7-CB; (**d**) V32-0.95-CB.

Figure 11 shows the optical microscopy images for the 32 MPa beams, revealing distinct corrosion characteristics at different stress levels. The dark regions represent the corrosion products, while the light regions indicate the intact wire material. The extent of corrosion increases with higher stress levels, as indicated by the larger dark regions in the higher-stressed samples.

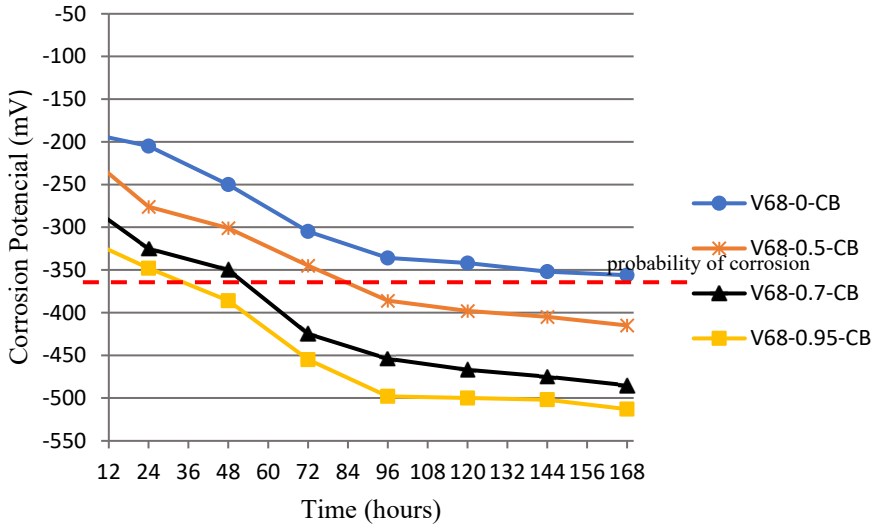


**Figure 12.** *Cont.*

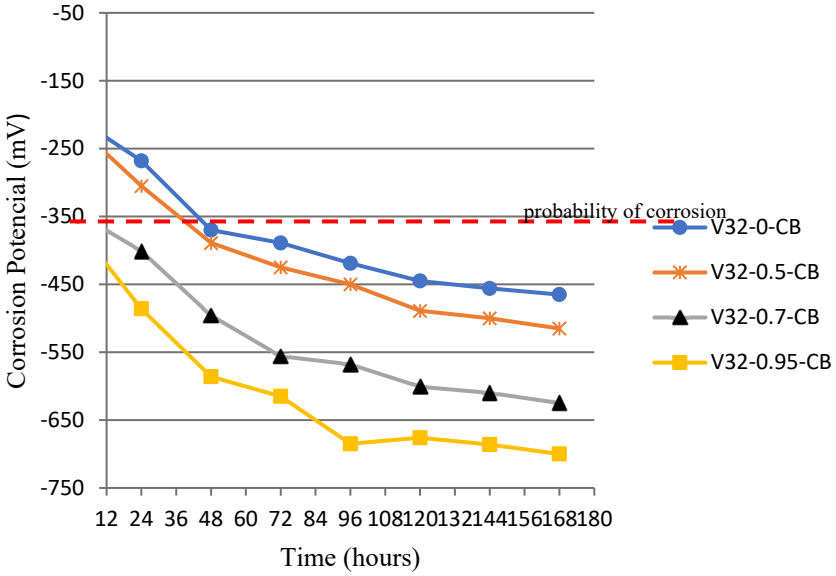


**Figure 12.** Corrosion potential (Ecorr) measurements for 68 MPa beams at various stress levels.

In contrast, Figure 12 shows the corrosion potential (Ecorr) for both 32 MPa and 68 MPa beams at various stress levels. For the 32 MPa beams, the corrosion potential readings indicate a higher susceptibility to corrosion compared to the 68 MPa beams. The Ecorr values for 32 MPa beams at 95% fptk pre-tension are significantly lower, indicating a more advanced corrosion state.

After an optical analysis, confocal microscopy offered a clearer view of corrosion morphology, detailing oxide layer thickness variations across different wire stress levels, especially between 70 and 95% fptk in 32 MPa beams (Table 3).

**Table 3.** Oxide layer measurement.

| Samples | Oxide Layer on the Surface of the Corroded Wire (μm) |
|---|---|
| V32-0-CB | 67.169 |
| V32-0.5-CB | 104.402 |
| V32-0.7-CB | 119.115 |
| V32-0.95-CB | 154.919 |

The final characterization phase used SEM analyses for a detailed, magnified view of wire surfaces, focusing on beams with pronounced corrosion (Figure 13). SEM revealed microstructural changes, corrosion patterns, and variations in porosity and corrosion product concentration, particularly in highly corroded beams like V32-0.5-CB, highlighting the advanced corrosion stage and stress-related surface cracks.

These metallographic analyses collectively provided a comprehensive understanding of the corrosion mechanisms at play. They revealed how different stress levels and environmental conditions influenced the corrosion behavior of the prestressed wires. This detailed examination was crucial for correlating the macroscopic behavior observed in the bending tests with the microscopic changes occurring in the material, thereby contributing significantly to the overall findings of the study (Figure 14).

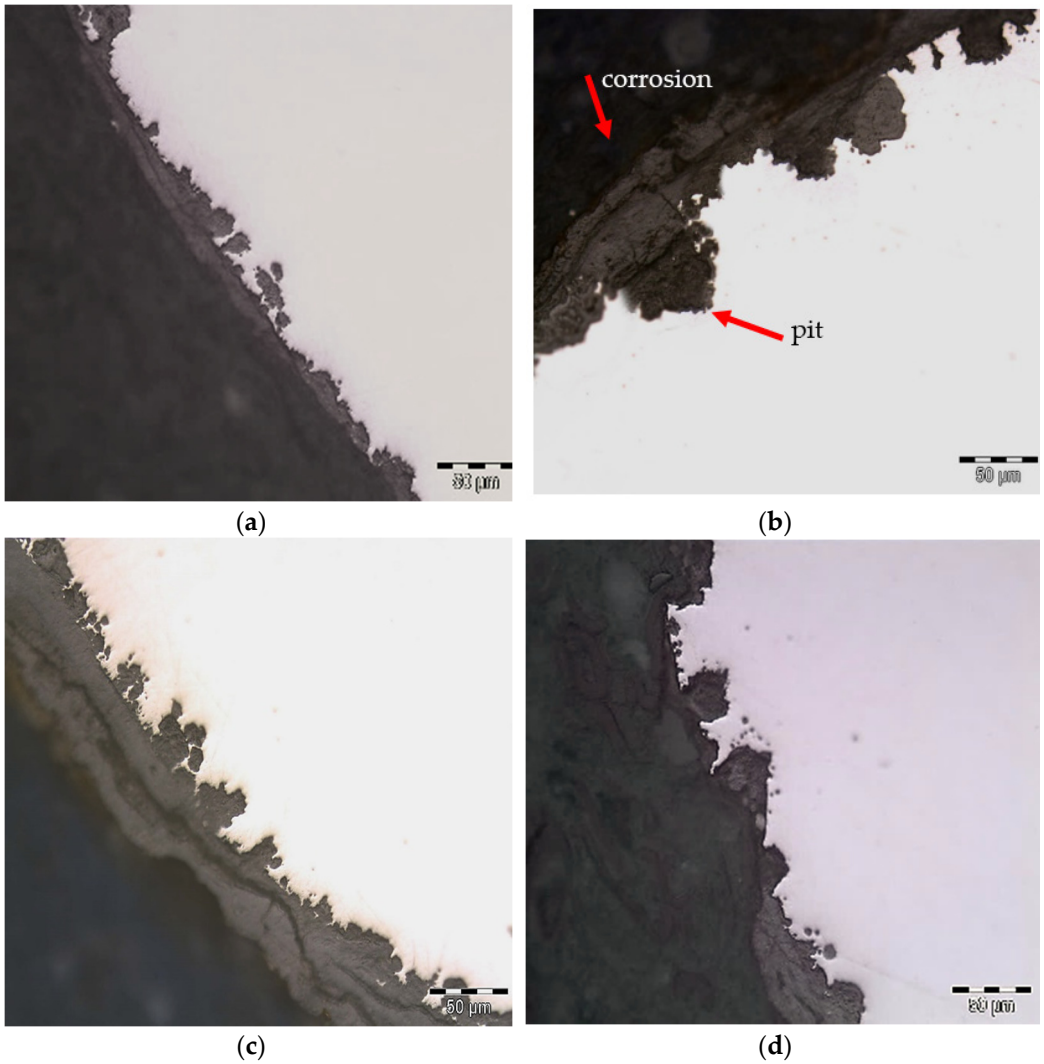


**Figure 13.** Appearance of the corroded wire cross-section: (**a**) V32-0-CB; (**b**) V32-0.5-CB; (**c**) V32-0.7-CB and (**d**) V32-0.95-CB, 400× magnification.

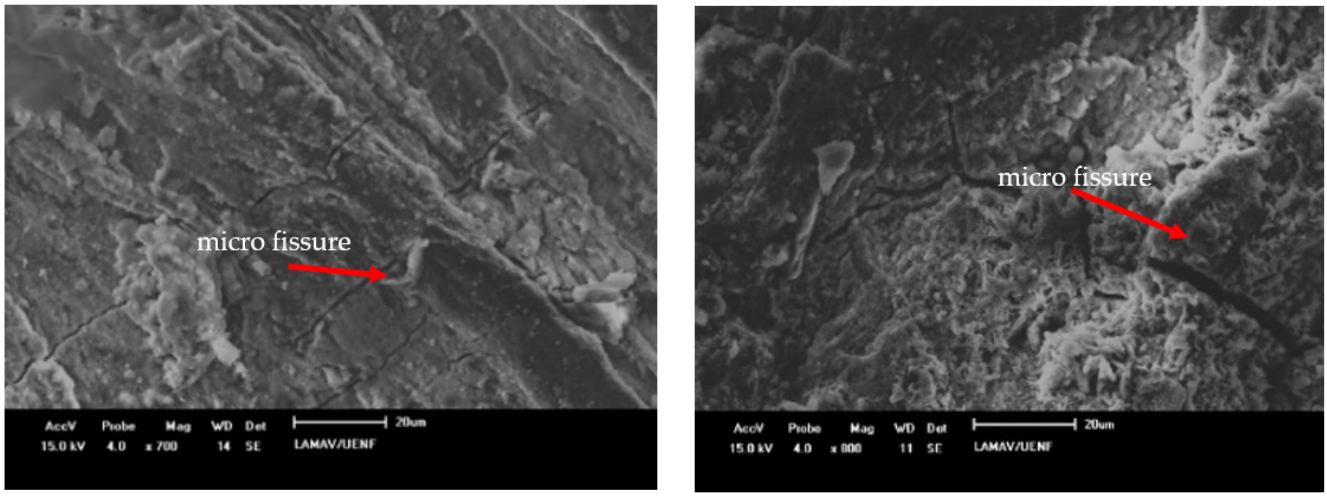


**Figure 14.** Details of the wires extracted from the fck 32 MPa beams, after cleaning.

### *4.8. Statistical and Machine Learning Analysis*

This study employed advanced statistical and machine learning techniques to develop predictive models for the ultimate bending moment of prestressed concrete beams. The primary focus was on understanding the impact of concrete strength, reinforcement strength, and corrosion on the structural integrity of these beams.

A statistical analysis methodology was designed for thorough interpretation and validation of data from both experimental and computational phases of the research. Initially, the analysis involves an extensive data collection process, gathering data from various sources, including material property measurements, corrosion rate assessments, beam deformation metrics, and computational model outputs. After data collection, data preparation focused on accuracy and completeness. This involved identifying and correcting any errors or inconsistencies in the data, converting the data into a format suitable for analysis through normalization or categorization, and identifying and understanding data points that significantly differ from the rest of the data set.

Descriptive statistics provided a preliminary overview of the data, which was critical for establishing a baseline understanding [32]. This includes calculating the average, median, and mode to identify the central value in the data, as well as assessing the spread or dispersion of the data through standard deviation and variance. The distribution of the data was analyzed using histograms and box plots to understand its shape and spread.

The inferential statistics stage applied statistical methods to infer properties about a population based on sampled data. This includes conducting tests like *t*-tests, chi-square tests, or ANOVA, depending on the type of data type, to assess statistical significance. Regression analysis, both linear and nonlinear, was employed to understand relationships between variables such as concrete strength, corrosion rate, and the material's properties. The correlation analysis measured the strength and direction of relationships between important variables.

For the complex data (increasing corrosion rate), advanced statistical techniques were used, including multivariate analysis methods like principal component analysis or factor analysis, to understand the structure of complex data sets, while time-series analysis methods like ARIMA models were used to understand temporal trends and patterns. Python's statistical libraries were used for these analyses, offering functionalities for complex calculations, graphical data representation, and model building.

In the final phase, the outcomes of the statistical analyses were interpreted in relation to the research objectives. This includes contextualizing the results within the broader context of the study's goals, identifying key patterns, trends, and anomalies, and discussing the implications of the statistical results for understanding corrosion in prestressed concrete structures.

Throughout the process, measures were taken to ensure the rigor and reliability of the statistical analysis. This includes verifying the validity of the assumptions underlying each statistical method, identifying and reporting potential errors or uncertainties in the analysis, and maintaining a transparent approach to ensure the replicability of the analysis by other researchers. This detailed and methodical approach aims to provide a deep and accurate interpretation of the data, supporting the research findings with robust statistical evidence.

Statistical Exploratory Data Analysis of Concrete Beam Data

To complement the experimental investigation of corrosion in prestressed concrete beams, we employed statistical and machine learning techniques to analyze the relationship between key variables and predict the structural integrity of the beams. These techniques provide a robust framework for understanding complex interactions and enhancing predictive accuracy.

Exploratory data analysis (EDA) is an indispensable phase in the data analysis process, laying the groundwork for subsequent statistical analysis. It involves a range of techniques

aimed at understanding the distributions of variables, detecting outliers, uncovering patterns, and identifying relationships between variables within a dataset.

Through graphical representations such as histograms, box plots, scatter plots, and more sophisticated visualizations (as used in this methodology), EDA provides a visual insight into the data, offering an intuitive understanding of its main characteristics. Summary statistics further complement this by quantifying central tendencies, dispersion, and other key attributes.

EDA is a continuous process, guiding and informing the modeling choices, hypothesis formulation, and data preprocessing decisions. Its iterative nature helps in refining research questions, validating assumptions, and ensuring that the conclusions drawn are based on a comprehensive and nuanced understanding of the data's underlying structure.

Exploratory data analysis (EDA) is an indispensable phase in the data analysis process, setting the stage for subsequent statistical analysis. It employs a range of techniques aimed at understanding variable distributions, detecting outliers, uncovering patterns, and identifying relationships within a dataset. Through graphical representations such as histograms, box plots, scatter plots, and sophisticated visualizations, as implemented in the current analysis, EDA offers visual insight into the data, providing an intuitive grasp of its main characteristics. Summary statistics complement these visual insights by quantifying central tendencies, dispersion, and other key attributes.

EDA is not just a preliminary step but a continuous process that guides and informs modeling choices, hypothesis formulation, and data preprocessing decisions. Its iterative nature aids in refining research questions, validating assumptions, and ensuring that conclusions are drawn from a comprehensive and nuanced understanding of the data's underlying structure.

Transitioning from theory to practice, the code for our EDA follows a structured approach. It begins by setting up a DataFrame with sample data on concrete beams, detailing attributes like concrete strength, reinforcement strength, corrosion rate, and bending moment. This DataFrame, named merged_df, serves as the basis for all subsequent analyses. Initially, the code calculates basic statistics such as the mean and standard deviation for all numerical columns in the DataFrame, providing an initial quantitative understanding of each variable.

The code then presents the frequency of different values through histograms for each numerical variable, helping visualize data distribution. It assesses the relationships between variables using a correlation matrix visualized as a heatmap, making it easier to see any strong relationships or patterns. To identify outliers or unusual values, the code generates boxplots for each numerical variable. These boxplots effectively display the median, quartiles, and potential outliers, offering a visual means to identify data points that stand out.

Further, the code extracts additional information from the 'Beam_ID' column, specifically the prestress level and corrosion status, adding these as new columns to the DataFrame. For a deeper analysis, it runs two statistical tests: an independent *t*-test and a Mann-Whitney U test. These tests determine if the differences in bending moments between corroded and non-corroded beams are statistically significant. The code calculates the average bending moments for both groups and presents them along with the test results, indicating the significance of the differences.

Finally, the algorithm visualizes the data by creating boxplots to compare bending moments between corroded and non-corroded beams, as well as a scatter plot to examine the relationship between prestress level and the ultimate bending moment while considering the corrosion status. This approach combines statistical calculations and visualizations to thoroughly explore and understand the dataset, paving the way for informed modeling and analysis.

The pseudocode that presents the EDA developed using this methodology can be seen in Algorithm 1.

**Algorithm 1** Statistical Analysis of Concrete Beam Data

```
Import pandas numpy seaborn matplotlib.pyplot
# Create a DataFrame with sample data
Initialize data with Beam ID, Concrete strength, etc.
Create DataFrame merged_df from data
# Descriptive Statistics
Print descriptive statistics of merged_df
# Distribution Analysis
Define numerical columns
Plot histograms for each numerical column in merged_df
# Correlation Analysis
Select numerical columns from merged_df
Calculate correlation matrix
Print correlation matrix
Plot heatmap of correlation matrix
# Outlier Detection
Plot boxplots for each numerical column
# Extract prestress level and corrosion status
Extract Prestress_Level from Beam_ID
Extract Corrosion_Status from Beam_ID
Print updated DataFrame
# Statistical Tests
Import ttest_ind, mannwhitneyu from scipy.stats
Separate ultimate moments based on corrosion status
Print mean values for non-corroded and corroded moments
Perform t-test and Mann-Whitney U test
Print p-values of the tests
# Data Visualization
Plot boxplots for bending moments based on corrosion status
Plot scatter plot for relationship between prestress level and ultimate bending moment
```

The process to develop a predictive model of concrete beam strength begins with creating a DataFrame using CSV files containing detailed attributes of concrete beams. These attributes include concrete strength, reinforcement strength, corrosion rate, and the ultimate bending moment, which is the primary variable of interest, indicating the structural integrity and safety of the beams. The initial step involves merging data from different sources based on a common 'Beam_ID', ensuring a comprehensive dataset for analysis (Figure 15).

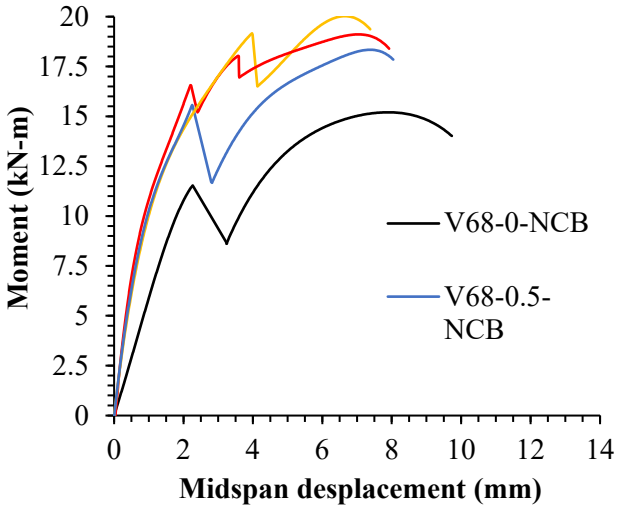


**Figure 15.** Vertical displacement at the center of the span of the non-corroded 68 MPa beams.

To capture the complex relationships and physical characteristics influencing beam strength, new features 'A', 'B', 'C', and 'D' are engineered and are written as,

$$Q = T_{corr} + 1$$

$$A = {f_c}^{2/3}$$

$$B = f_{py}/Q$$

$$C = f_{ptk}/Q$$

$$D = -T_{corr}$$

where

$T_{corr}$ represents the adjusted corrosion rate, being the average corrosion rate measured in mm/year from the dataset;

$f_c$ is the concrete strength at 28 days;

$f_{py}$ is the yield steel resistance from the prestressed reinforcement;

$f_{ptk}$ is the prestressed applied in the reinforcement;

These features are derived using domain-specific transformations that reflect how various factors, like concrete strength, reinforcement tension, and corrosion rates, interact to affect the beam's bending moment. Standardizing these features is crucial for effective modeling, especially given the wide range of data. Therefore, the StandardScaler is employed to normalize the features, removing the mean and scaling them to unit variance.

The core of the predictive analysis is built on two regression techniques: linear regression and lasso regression. Linear regression is implemented to model the linear relationship between the engineered features and the ultimate bending moment. To assess the model's robustness and its ability to generalize to unseen data, 10-fold cross-validation is performed using cross_val_score, providing a reliable estimate of the model's predictive performance.

Evaluating the model's accuracy and fit is essential. The mean squared error (MSE) and $R^2$ were calculated for the linear regression model. The MSE provides a measure of the average squared difference between the observed actual outcomes and the model's predictions, with a lower value indicating a better fit. On the other hand, $R^2$ indicates the proportion of variance in the ultimate bending moment that is predictable from the features, with a higher value suggesting a better explanatory model.

To enhance the model and potentially reduce overfitting, a lasso regression was also used. Lasso introduces regularization to the model, adding a penalty equivalent to the absolute value of the magnitude of the coefficients. This not only helps prevent overfitting but also performs feature selection by shrinking some coefficients to zero. A range of alpha values (regularization strengths) was considered, and GridSearchCV was employed to find the optimal alpha that balances model complexity and accuracy. The best Lasso model is then evaluated, calculating its MSE and $R^2$ to understand its performance.

The equations representing the predicted ultimate bending moment for both the linear and lasso regression models were developed. These equations highlight the influence of each feature on the predicted outcome, offering insights into the underlying physical phenomena. The performance metrics and regression equations are presented, providing a comprehensive overview of the models' predictive capabilities and the relative importance of each feature in determining the ultimate bending moment of concrete beams.

$$
\begin{aligned}
&\textit{AverageMSE} : 2.426\\
&\textit{Standard deviation of MSE} : \ 2.580\\
&\textit{Best alpha} : \ 0.013\\
&\textit{Best MSE} : \ 1.505\\
&\textit{Lasso regression MSE} : \ 0.517\\
&\textit{Lasso regression R2} : \ 0.905\\
&\textit{Predicted ultimate bending moment} :\\
&\quad = 16.13 + (0.63 \times A) + (1.31 \times B) + (1.12 \times C)\\
&\quad + (0.21 \times D)
\end{aligned}
$$

Through this methodical approach, this study predicted the structural behavior of concrete beams under corrosion condition as can be seen below.

$$P_u = 16.13 + \frac{1.31 \times \sqrt{f_{py}} + 1.12 \times f_{ptk}}{(T_{corr} + 1)} 0.63 \times {f_c}^{2/3} - 0.21 \times T_{corr}$$

The pseudocode for the ultimate bending moment prediction is presented in Algorithm 2.

**Algorithm 2** Pseudocode for Ultimate Bending Moment Prediction with Linear and Lasso Regression

**IMPORT** libraries
**LOAD** the CSV files into properties_df and ultimate_df
**MERGE** the dataframes on 'Beam_ID'into merged_df
**DEFINE** new feature Q in merged_df
**CALCULATE** new features A, B, C, and D in merged_df
**PREPARE** the dataset for the model with features ['A','B','C','D'] and target 'actual_ultimate_bending_moment(kN.m)'
**SCALE** the features using StandardScaler
**procedure** TRAINLINEARREGRESSION(X,y)
    Initialize LinearRegression model
    Calculate cross-validation scores
    Fit the model on X and y
    Predict and calculate MSE and R2
    Verify Linear Regression MSE, R2, and the equation
    Verify Average MSE and Standard Deviation of MSE from cross-validation
**end procedure**
**procedure** TRAINLASSOREGRESSION(X,y)
    Initialize Lasso model with a range of alphas
    Perform GridSearchCV to find the best alpha
    Fit the model with the best alpha on X and y
    Predict and calculate MSE and R2
    Verify Lasso Regression MSE, R2, and the equation
**end procedure**
**MAIN**
X← scaled features, y← target values
TRAINLINEARREGRESSION(X,y)
TRAINLASSOREGRESSION(X,y)
**END**

Experimental results served as the training data for the machine learning models. For example, the corrosion rates measured during the experiments were used to train the models to predict the ultimate bending moment. This integration ensures that the models are grounded in empirical evidence.

## 5. Results

This study investigated the effects of corrosion on prestressed concrete beams with 5 mm diameter wires, revealing key insights. Detailed in Tables 4 and 5, the results indicate the complex interplay between corrosion, concrete strength, and prestressing levels, significantly impacting structural integrity.

**Table 4.** Corrosion rate results.

| Samples | Attack Time (hours) | Mass Loss (%) | Corrosion Rate (mm/year) |
|---|---|---|---|
| V32-0-CB | 168 | 4.63 | 0.37 |
| V32-0.5-CB | | 5.75 | 0.46 |
| V32-0.7-CB | | 6.98 | 0.55 |
| V32-0.95-CB | | 8.01 | 0.64 |
| V68-0-CB | | 2.56 | 0.20 |
| V68-0.5-CB | | 3.15 | 0.25 |
| V68-0.7-CB | | 4.32 | 0.35 |
| V68-0.95-CB | | 5.32 | 0.42 |

**Table 5.** Experimental $P_{fiss}$ and $P_{ult}$ values of the tested beams.

| Beam | Corroded | | Non-Corroded | |
|---|---|---|---|---|
| | $P_{fiss}$ (kN) | $P_{ult}$ (kN) | $P_{fiss}$ (kN) | $P_{ult}$ (kN) |
| V32-0 | 32.76 | 42.99 | 31.03 | 34.86 |
| V32-0.5 | 36.56 | 50.16 | 34.71 | 38.21 |
| V32-0.7 | 38.20 | 51.59 | 35.48 | 39.08 |
| V32-0.95 | 40.78 | 54.21 | 31.50 | 35.76 |
| V68-0 | 33.87 | - | 32.53 | - |
| V68-0.5 | 41.00 | 52.29 | 40.50 | 43.83 |
| V68-0.7 | 45.26 | 52.96 | 44.06 | 47.91 |
| V68-0.95 | 54.86 | - | 51.36 | - |

Our findings, as shown in Table 4, demonstrate considerable corrosion rates across all sample groups, with a greater impact in beams under higher pre-tension. An ANOVA with a 5% significance level confirmed the substantial influence of stress on wire weight loss, suggesting that corrosion accelerated under conditions of increased stress. This phenomenon is partly due to decreased capillary porosity in stronger beams, which impedes oxygen flow and exacerbates the corrosion process.

Deflection versus load-like curves (Figures 8 and 10, and Algorithm 1) offered critical insights into the beams' structural behavior under load. Intriguingly, both corroded and non-corroded prestressed beams displayed similar displacement patterns pre-flexural cracking, implying that initial stiffness is largely unaffected by corrosion. However, a marked decline in post-cracking stiffness and load-bearing capacity was observed with increased corrosion, as higher corrosion rates significantly reduced post-cracking stiffness, highlighting the detrimental impact of corrosion on structural performance.

The bond strength between steel wires and concrete, crucial for structural integrity, deteriorated with corrosion. This was evidenced by the kinematics of critical flexural crack openings (Figures 7 and 9), where corroded beams reached ultimate tensile stress quicker than non-corroded ones, resulting in premature cracking. The compromised bond strength and loss of prestressing due to corrosion culminated in more extensive crack openings

and reduced overall structural integrity, with cracking patterns (Figure 10) showing more extensive propagation in corroded beams.

Table 5 presents a discernible decrease in the load-bearing capacity of corroded beams. Corroded V32 beams exhibited a 23% to 34% reduction in ultimate load compared to non-corroded ones, while V68 beams showed a 9.5% to 16% decline. This significant reduction is an important factor in the design and assessment of prestressed concrete structures, underscoring the urgency for effective corrosion mitigation strategies.

The observed deformation patterns (Algorithm 1) and specific strain values at breaking load (Table 5) corroborate the loss of tensile strength in wires due to corrosion. This reduction in deformation capacity has profound implications for the durability and service life of prestressed concrete structures, emphasizing the need for designs that account for long-term corrosion impacts. Table 6 presents the specific strain of the reinforcement for each beam's ultimate load capacity.

**Table 6.** Specific strain of the reinforcement for ultimate load.

| Beam | Deformation (ε) (‰) |
|---|---|
| V32-0-NCB | 3.75 |
| V32-0.5-NCB | 3.5 |
| V32-0.7-NCB | 3.2 |
| V32-0.95-NCB | 2.9 |
| V32-0-CB | 3.4 |
| V32-0.5-CB | 3.15 |
| V32-0.7-CB | 2.8 |
| V32-0.95-CB | 2.3 |

Our findings underscore the critical importance of corrosion resistance in sustainable civil engineering practices. By enhancing our understanding of corrosion dynamics in prestressed structures, engineers can develop more resilient and durable designs, reducing the need for frequent repairs and replacements and, consequently, minimizing the environmental footprint of construction activities.

Incorporating statistical and machine learning analyses, we've identified a consistent decrease in load-bearing capacity and tensile strength in corroded beams. This predictive insight, derived from a rigorous data-driven approach, not only validates our experimental observations but also provides a quantitative framework for assessing and mitigating corrosion impact in prestressed concrete structures.

Correlation analyses revealed strong links between corrosion rates and ultimate bending moments. Higher corrosion rates were associated with lower bending moments, indicating a detrimental effect of corrosion on structural integrity.

The linear regression model achieved an $R^2$ of 0.86, indicating a strong linear relationship between the input features and the predicted bending moment. The lasso regression model further improved accuracy, with an $R^2$ of 0.905 and reduced MSE.

These results not only highlight the need for effective corrosion mitigation strategies but also pave the way for future research and development in corrosion-resistant materials and design practices. Our study contributes to a more sustainable and resilient built environment, aligning with global efforts to enhance infrastructure service life and performance.

## 6. Discussion

This study developed a novel predictive model to quantify the impact of corrosion on prestressed concrete beams, focusing on the relationship between stress levels, corrosion rates, and concrete strength. Through rigorous empirical analysis and advanced machine

learning algorithms, the model provides a robust numerical equation to assess structural integrity and service life of prestressed concrete beams, marking a significant advancement in civil engineering.

The simulation conducted in the laboratory focused primarily on chloride-induced corrosion. Factors such as Mg, K, Ca, SO4 ions, dissolved oxygen, marine organisms, temperature, hydrostatic pressure, and tidal action were not included. These additional variables significantly impact corrosion and should be considered in future studies for a more comprehensive simulation. The model accurately integrates variables such as concrete strength ($fc$), yield strength of prestressed reinforcement ($fpy$), prestress applied ($fpt$), and average corrosion rate ($Tcorr$) to predict the ultimate bending moment ($Pu$).

The empirical analysis revealed that higher stress levels and concrete strengths significantly influence corrosion rates and structural integrity. Beams with 95% prestress level exhibited a corrosion rate of 0.64 mm/year, compared to 0.37 mm/year for non-prestressed beams, indicating that higher prestress levels exacerbate the corrosion process. These findings are consistent with previous studies that highlight the vulnerability of prestressed concrete in chloride environments.

Digital image correlation (DIC) provided insights into deformation and crack patterns, showing significant reductions in post-cracking stiffness and load-bearing capacity in corroded beams. For instance, the ultimate load capacity of 32 MPa beams decreased by 23% to 34% due to corrosion, while 68 MPa beams showed a reduction of 9.5% to 16%. These results underscore the critical importance of monitoring and maintaining prestressed concrete structures in corrosive environments.

The machine learning-based predictive model achieved a mean squared error of 0.517 and an $R2$ value of 0.905, indicating high accuracy in predicting the ultimate bending moment of corroded beams. This capability can significantly enhance corrosion risk assessment and management in coastal infrastructure. The model's practical application lies in its ability to inform maintenance schedules and assess the remaining service life of existing structures.

The statistical and machine learning analysis confirms the significant impact of corrosion on the structural integrity of prestressed concrete beams. The predictive models developed provide a valuable tool for assessing the potential degradation of such structures over time, enabling more proactive maintenance strategies.

Our findings highlight the need for regular maintenance and inspection of pre-stressed concrete structures in corrosive environments. The predictive models developed can serve as a basis for creating maintenance schedules and assessing the remaining service life of existing structures.

Future research should refine the model by incorporating additional environmental factors like temperature and humidity. Exploring advanced materials and coatings to mitigate corrosion in prestressed concrete structures would also be beneficial. Integrating real-time monitoring systems with predictive analytics could further enhance the durability and safety of coastal infrastructure.

By enhancing our understanding of corrosion dynamics and developing predictive tools, this research contributes to more resilient and durable construction practices, ultimately supporting the goal of sustainable infrastructure development.

## 7. Conclusions

This study introduced a novel predictive model to quantify the impact of corrosion on prestressed concrete beams, emphasizing the intricate relationship between stress levels, corrosion rates, and concrete strength. Developed through rigorous empirical analysis combined with advanced machine learning algorithms, the model provides a robust numerical equation to assess structural integrity and service life, representing a significant analytical advancement in civil engineering. By enhancing our understanding of corrosion dynamics and developing predictive tools, this research contributes to more resilient and durable construction practices, ultimately supporting the goal of sustainable infrastruc-

ture development. The model's technical accuracy and precision are its core strengths, effectively integrating complex variable relationships into a practical tool for industry professionals. This development marks a step forward in predictive analytics for assessing the degradation of prestressed concrete structures. The formula used to predict the ultimate bending moment (Pu) is given by

$$Pu = 16.13 + Tcorr + 11.31 \times fpy + 1.12 \times fptk + 0.63 \times fc2/3 \\ -0.21 \times Tcorr$$

The empirical analysis revealed that higher stress levels and concrete strengths significantly influence corrosion rates and the structural integrity of the beams. The ultimate load capacity of beams with higher prestress levels exhibited significant reductions due to corrosion, highlighting the importance of regular maintenance and proactive measures. For instance, Figure 11 shows the optical microscopy images for the 32 MPa beams, revealing distinct corrosion characteristics at different stress levels. In Figure 12, the corrosion potential (Ecorr) readings for both 32 MPa and 68 MPa beams indicate varying susceptibility to corrosion, with 32 MPa beams showing higher corrosion rates at 95% fptk pre-tension.

These findings underscore the need for effective corrosion mitigation strategies and provide a quantitative framework for assessing and managing the risk of corrosion in prestressed concrete structures. Future research should focus on refining the model and exploring innovative materials and monitoring techniques to enhance the durability and sustainability of coastal infrastructure. The findings also demonstrated pronounced corrosion rates across all sample groups, with an accentuated effect in beams under higher pre-tension, as detailed in Tables 4 and 5. The detailed analysis of deflection versus load-like curves (Figures 8 and 10, and Algorithm 1) offered critical insights into the beams' structural behavior under load, highlighting the accelerated corrosion in higher stressed beams and the corresponding reduction in structural integrity.

The machine learning analysis demonstrates the effectiveness of integrating statistical and machine learning techniques with experimental data to predict the impact of corrosion on structural integrity. Future research should explore additional environmental factors and advanced modeling techniques to further enhance predictive accuracy.

The bond strength between steel wires and concrete, crucial for structural integrity, deteriorated with corrosion. The kinematics of critical flexural crack opening (Figures 7 and 9) showed that corroded beams reached ultimate tensile stress quicker than non-corroded ones, resulting in premature cracking. The compromised bond strength and loss of prestressing due to corrosion culminated in more extensive crack openings and reduced overall structural integrity.

Future research should focus on refining these predictive models and investigating novel approaches to addressing the pervasive challenge of corrosion in corrosive environments. By continuing to improve the model's precision and applicability, the field can progress toward more durable and sustainable construction practices, ultimately enhancing the service life and safety of coastal infrastructure.

**Author Contributions:** Conceptualization, R.M.R.P., K.F., B.B.F.d.C., M.A., M.K.N., S.G., D.K., and A.H.; methodology, R.M.R.P., K.F., S.G., D.K., and A.H.; software, R.M.R.P., K.F., S.G., and A.H.; validation, R.M.R.P., K.F., B.B.F.d.C., M.A., M.K.N., S.G., D.K., and A.H.; formal analysis, R.M.R.P., K.F., B.B.F.d.C., M.A., M.K.N., and S.G.; investigation, R.M.R.P., S.G., and A.H.; resources, R.M.R.P., D.K., K.F., B.B.F.d.C., M.A., M.K.N., S.G., and A.H.; methodology, R.M.R.P., K.F., S.G., and A.H.; data curation, R.M.R.P. and K.F.; writing—original draft preparation, R.M.R.P., K.F., S.G., and A.H.; writing—review and editing, R.M.R.P., K.F., B.B.F.d.C., M.A., M.K.N., S.G., and A.H.; visualization, R.M.R.P., S.G., and A.H.; supervision, S.G. and A.H.; project administration, R.M.R.P., K.F., S.G., D.K., and A.H. All authors have read and agreed to the published version of the manuscript.

**Funding:** This research was funded by Coordenação de Aperfeiçoamento de Pessoal de Nível Superior grant number 88881.846502/2023-01.

**Informed Consent Statement:** Not applicable.

**Data Availability Statement:** Data may be obtained upon reasonable request.

**Acknowledgments:** The authors would like to acknowledge the support of Conselho Nacional de Desenvolvimento Científico e Tecnológico (CNPq 304726/2021-4) and Fundação Carlos Chagas Filho de Amparo à Pesquisa do Estado do Rio de Janeiro (FAPERJ E-26400.205.206/2022(284891)) and (FAPERJ E-26/210.950/2024 (295973)), and CAPES Finance Code 01, which helped in the development of this research.

**Conflicts of Interest:** The authors declare no conflicts of interest.

## References

1. Meng, Z.; Liu, Q.F.; Xia, J.; Cai, Y.; Zhu, X.; Zhou, Y.; Pel, L. Mechanical–Transport–Chemical Modeling of Electrochemical Repair Methods for Corrosion-Induced Cracking in Marine Concrete. *Comput.-Aided Civ. Infrastruct. Eng.* **2022**, *37*, 1854–1874. [CrossRef]
2. Liu, Q.F.; Iqbal, M.F.; Yang, J.; Lu, X.Y.; Zhang, P.; Rauf, M. Prediction of Chloride Diffusivity in Concrete Using Artificial Neural Network: Modelling and Performance Evaluation. *Constr. Build. Mater.* **2021**, *268*, 121082. [CrossRef]
3. Aljibori, H.S.; Alamiery, A.; Kadhum, A.A.H. Advances in Corrosion Protection Coatings: A Comprehensive Review. *Int. J. Corros. Scale Inhib.* **2023**, *12*, 1476–1520. [CrossRef]
4. Cabrera, J. Deterioration of Concrete Due to Reinforcement Steel Corrosion. *Cem. Concr. Compos.* **1996**, *18*, 47–59. [CrossRef]
5. Bertolini, L. Steel Corrosion and Service Life of Reinforced Concrete Structures. *Struct. Infrastruct. Eng.* **2008**, *4*, 123–137. [CrossRef]
6. Jiang, T.; Kong, Q.; Peng, Z.; Wang, L.; Dai, L.; Feng, Q.; Huo, L.; Song, G. Monitoring of Corrosion-Induced Degradation in Prestressed Concrete Structure Using Embedded Piezoceramic-Based Transducers. *IEEE Sens. J* **2017**, *17*, 5823–5830. [CrossRef]
7. McDonald, D.B. Corrosion Protection for Concrete Structures in Marine Environments. Coastal Engineering Practice. In Proceedings of the 2011 Conference on Coastal Engineering Practice, San Diego, CA, USA, 21–24 August 2011; pp. 78–88. [CrossRef]
8. Bender, R.; Féron, D.; Mills, D.; Ritter, S. Corrosion Challenges towards a Sustainable Society. *Mater. Corros.* **2022**, *73*, 1730–1751. [CrossRef]
9. Verma, C.; Ebenso, E.; Quraishi, M. Ionic Liquids as Green and Sustainable Corrosion Inhibitors for Metals and Alloys: An Overview. *J. Mol. Liq.* **2017**, *233*, 403–414. [CrossRef]
10. Li, F.; Yuan, Y.; Li, C. Corrosion Propagation of Prestressing Steel Strands in Concrete Subject to Chloride Attack. *Constr. Build. Mater.* **2011**, *25*, 3878–3885. [CrossRef]
11. Darmawan, M.S. Pitting Corrosion Model for Partial Prestressed Concrete (Pc) Structures in a Chloride Environment. *IPTEK J. Technol. Sci.* **2009**, *20*, 78–88. [CrossRef]
12. Funahashi, M. Predicting Corrosion-Free Service Life of a Concrete Structure in a Chloride Environment. *Materials* **1990**, *87*, 581–587. [CrossRef] [PubMed]
13. Nguyen, T.H.Y.; Tran, V.M.; Pansuk, W.; Cao, N.T.; Bui, V.H.L. Electrochemical Chloride Extraction on Reinforced Concrete Contaminated External Chloride: Efficiencies of Intermittent Applications and Impacts on Hydration Products. *Cem. Concr. Compos.* **2021**, *121*, 104076. [CrossRef]
14. Kanagaraj, B.; Priyanka, R.; Anand, N.; Kiran, T.; Andrushia, A.D.; Lubloy, E. A Sustainable Solution for Mitigating Environmental Corrosion in the Construction Sector and Its Socio-Economic Concern. *Case Stud. Constr. Mater.* **2024**, *20*, e03089. [CrossRef]
15. Lu, Z.H.; Zhou, Q.H.; Li, H.; Zhao, Y.G. A New Empirical Model for Residual Flexural Capacity of Corroded Post-Tensioned Prestressed Concrete Beams. *Structures* **2021**, *34*, 4308–4321. [CrossRef]
16. Minh, H.; Mutsuyoshi, H.; Niitani, K. Influence of Grouting Condition on Crack and Load-Carrying Capacity of Post-Tensioned Concrete Beam Due to Chloride-Induced Corrosion. *Constr. Build. Mater.* **2007**, *21*, 1568–1575. [CrossRef]
17. Coronelli, D.; Castel, A.; Vu, N.A.; François, R. Corroded Post-Tensioned Beams with Bonded Tendons and Wire Failure. *Eng. Struct.* **2009**, *31*, 1687–1697. [CrossRef]
18. Zhang, X.; Wang, L.; Zhang, J.; Ma, Y.; Liu, Y. Flexural Behavior of Bonded Post-Tensioned Concrete Beams under Strand Corrosion. *Nucl. Eng. Des.* **2017**, *313*, 414–424. [CrossRef]
19. Hussain, R. Modeling of Corrosion; Steel, Concrete and Environment. *J. Civ. Environ. Eng.* **2014**, *4*, 1–5. [CrossRef]
20. Shafei, B.; Alipour, A.; Shinozuka, M. Prediction of Corrosion Initiation in Reinforced Concrete Members Subjected to Environmental Stressors: A Finite-element Framework. *Cem. Concr. Res.* **2012**, *42*, 365–376. [CrossRef]
21. Taffese, W.Z.; Sistonen, E. Machine Learning for Durability and Service-Life Assessment of Reinforced Concrete Structures: Recent Advances and Future Directions. *Autom. Constr.* **2017**, *77*, 1–14. [CrossRef]
22. Elfergani, H.A.; Pullin, R.; Holford, K.M. Damage Assessment of Corrosion in Prestressed Concrete by Acoustic Emission. *Constr. Build. Mater.* **2013**, *40*, 925–933. [CrossRef]
23. Shevtsov, D.; Cao, N.L.; Nguyen, V.C.; Nong, Q.Q.; Le, H.Q.; Nguyen, D.A.; Zartsyn, I.; Kozaderov, O. Progress in Sensors for Monitoring Reinforcement Corrosion in Reinforced Concrete Structures—A Review. *Sensors* **2022**, *22*, 3421. [CrossRef] [PubMed]
24. Wang, Y.; Pan, Z.; Zhao, C.; Zeng, B. Long-Term Behavior of Prestressed Concrete Industrial Buildings in Chloride-Based Industrial Environments. *J. Build. Eng.* **2023**, *76*, 107344. [CrossRef]

25. Robles, K.P.V.; Gucunski, N.; Kee, S.H. Evaluation of Steel Corrosion-Induced Concrete Damage Using Electrical Resistivity Measurements. *Constr. Build. Mater.* **2024**, *411*, 134512. [CrossRef]
26. Angst, U. Challenges and Opportunities in Corrosion of Steel in Concrete. *Mater. Struct.* **2018**, *51*, 4. [CrossRef]
27. Apostolopoulos, C. The Consequences of Chloride-Induced Corrosion on Steel Bar and Reinforced Concrete Structures. *J. Appl. Mech. Eng.* **2012**, *1*, e109. [CrossRef]
28. Pavlakovic, B.; Lowe, M.; Cawley, P. Guided Ultrasonic Waves for the Inspection of Post-Tensioned Bridges. In *Review of Progress in Quantitative Nondestructive Evaluation*; Springer: New York, NY, USA, 1998; pp. 1557–1564. [CrossRef]
29. Dai, L.; Wang, L.; Zhang, J.; Zhang, X. A Global Model for Corrosion-Induced Cracking in Prestressed Concrete Structures. *Eng. Fail Anal.* **2016**, *62*, 263–275. [CrossRef]
30. Lee, B.; Koh, K.-T.; Ismail, M.; Ryu, H.-S.; Kwon, S.-J. Corrosion and Strength Behaviors in Prestressed Tendon under Various Tensile Stress and Impressed Current Conditions. *Adv. Mater. Sci. Eng.* **2017**, *2017*, 1–7. [CrossRef]
31. Lu, Z.-H.; Wang, H.; Qu, F.; Zhao, Y.-G.; Li, P.; Li, W. Novel Empirical Model for Predicting Residual Flexural Capacity of Corroded Steel Reinforced Concrete Beam. *Front. Struct. Civ. Eng.* **2020**, *14*, 888–906. [CrossRef]
32. Jia, H.; Qiao, G.; Han, P. Machine Learning Algorithms in the Environmental Corrosion Evaluation of Reinforced Concrete Structures—A Review. *Cem. Concr. Compos.* **2022**, *133*, 104725. [CrossRef]


**Disclaimer/Publisher's Note:** The statements, opinions and data contained in all publications are solely those of the individual author(s) and contributor(s) and not of MDPI and/or the editor(s). MDPI and/or the editor(s) disclaim responsibility for any injury to people or property resulting from any ideas, methods, instructions or products referred to in the content.